Proper Generalized Decomposition and layer-wise approach for the modeling of composite plate structures

P. Vidal, L. Gallimard, O. Polit

Proper Generalized Decomposition and layer-wise approach for the modeling of composite plate structures

P. Vidal *, L. Gallimard, O. Polit

Laboratoire Energétique, Mécanique, Electromagnétisme, Université Paris Ouest Nanterre-La Défense, 50 rue de Sèvres, 92410 Ville d'Avray, France

Keywords:
Composite structures
Sandwich
Finite element analysis
Proper Generalized Decomposition

A B S T R A C T

In the framework of the design of laminated and sandwich structures, the computation of local quantities needs a layer-wise approach. But, the computational cost of such approach increases with the number of layers. In this work, the introduction of the Proper Generalized Decomposition (PGD) is presented for the layer-wise modeling of heterogeneous structures in order to reduce the number of unknowns. The displacement field is approximated as a sum of separated functions of the in-plane coordinates x, y and the transverse coordinate z. This choice yields to an iterative process that consists of solving a 2D and 1D problem successively at each iteration. In the thickness direction, a fourth-order expansion in each layer is considered. For the in-plane description, classical Finite Element method is used.

After a preliminary study to show the relevance of the present approach, mechanical tests for thin to thick laminated and sandwich plates with various boundary conditions are presented. The results are compared with elasticity reference solutions.

1. Introduction

Composite and sandwich structures are widely used in the industrial field due to their excellent mechanical properties, especially their high specific stiffness and strength. In this context, they can be subjected to severe mechanical loads. For composite design, accurate knowledge of displacements and stresses is required. So, it is important to take into account effects of the transverse shear deformation due to the low ratio of transverse shear modulus to axial modulus, or failure due to delamination ... In fact, they can play an important role on the behavior of structures in services, which leads to evaluate precisely their influence on local stress fields in each layer, particularly on the interface between layers.

According to published research, various theories in mechanics for composite or sandwich structures have been developed. On the one hand, the Equivalent Single Layer approach (ESL) in which the number of unknowns is independent of the number of layers, is used. But, the transverse shear and normal stresses continuity on the interfaces between layers are often violated. We can distinguish the classical laminate theory (Tanigawa et al., 1989) (unsuitable for composites and moderately thick plates), the first order shear deformation theory (Yang et al., 1966), and higher order theories with displacement (Cook and Tessler, 1998; Kant and Swaminathan, 2002; Librescu, 1967; Lo et al., 1977; Matsunaga, 2002; Reddy, 1984; Whitney and Sun, 1973; Polit et al., 2012) and mixed (Carrera, 2000; Kim and Cho, 2007) approaches. On the other hand, the layerwise approach (LW) aims at overcoming the restriction of the ESL concerning the discontinuity of out-of-plane stresses on the interface layers and taking into account the specificity of layered structure. But, the number of dofs depends on the number of layers. We can mention the folllowing contributions (Ferreira, 2005; Icardi, 2001; Pagano, 1969; Reddy, 1989; Shimpi and Ainapure, 2001) within a displacement based approach and (Carrera, 1999, 2000; Rao and Desai, 2004) within a mixed formulation. As an alternative, refined models have been developed in order to improve the accuracy of ESL models avoiding the additional computational cost of LW approach. Based on physical considerations and after some algebraic transformations, the number of unknowns becomes independent of the number of layers. Whitney (1969) has extended the work of Ambartsumyan (1969) for symmetric laminated composites with arbitrary orientation and a quadratic variation of the transverse stresses in each layer. So, a family of models, denoted zig-zag models, was derived (see Kapuria et al., 2003; Lee et al., 1992; Sciuva and Icardi, 2001). Note also the refined approach based on the Sinus model (Vidal and Polit, 2008, 2009, 2011). This above literature deals with only some aspects of the broad research activity about models for layered structures and corresponding finite element formulations. An extensive assessment of different approaches has been made in Carrera, 2002, 2003; Noor and Burton, 1990; Reddy, 1997; Zhang and Yang, 2009.

Over the past years, the Proper Generalized Decomposition (PGD) has shown interesting features in the reduction model framework (Ammar et al., 2006). It has been used in the context

* Corresponding author. Tel.: +33 140974855.
E-mail address: philippe.vidal@u-paris10.fr (P. Vidal).

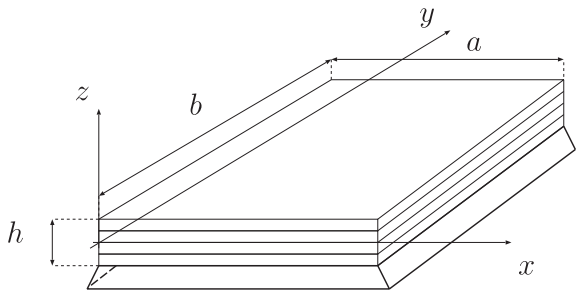

Fig. 1. The laminated plate and coordinate system.

of separation of coordinate variables in multi-dimensional PDEs (Ammar et al., 2006). And in particular, it has been applied for composite plates in Savoia and Reddy (1992) based on Navier-type solution and Bognet et al. (2012) using Finite Element (FE) method.

This work is based on the separation representation where the displacements are written under the form of a sum of products of bidimensional polynomials of (x,y) and unidimensional polynomials of z. In Bognet et al. (2012), a piecewise linear variation in the thickness direction is used, whereas in the present work, a piecewise fourth-order Lagrange polynomial of z is chosen. As far as the variation with respect to the in-plane coordinates is concerned, a 2D eight-node quadrilateral FE is employed. Using the PGD, each unknown function of (x,y) is classically approximated using one degree of freedom (dof) per node of the mesh and the LW unknown functions of z are global for the whole plate. Finally, the deduced non-linear problem implies the resolution of two linear problems alternatively. This process yields to a 2D and a 1D problems in which the number of unknowns is smaller than a classical layerwise approach. The interesting feature of this approach lies on the possibility to have a higher-order z-expansion and to refine the description of the mechanical quantities through the thickness without increasing the computational cost. This is particularly suitable for the modeling of composite structures.

We now outline the remainder of this article. First the mechanical formulation is given. Then, the principles of the PGD are briefly recalled in the framework of our study. The particular assumption on the displacements yields a non-linear problem. An iterative process is chosen to solve this one. The FE discretization is also described. Then, numerical tests are performed. A homogeneous case is first considered to compare the linear approach developed in Bognet et al. (2012) and the present fourth-order expansion with the same number of dofs. Different convergence studies are addressed. Then, the modeling of various laminated and sandwich plates under a global or localized pressure is addressed. The influence of the slenderness ratio is studied. The accuracy of the results is evaluated by comparisons with an exact 3D theory for laminates in bending (Pagano, 1970). A special attention is pointed towards the capacity of the approach to capture local effects and the evaluation of its range of validity. Finally, the computational complexity of the method is given and compared with classical layerwise approach.

2. Reference problem description

2.1. The governing equations

Let us consider a plate occupying the domain $\mathcal{V} = \Omega \times \Omega_z$ with $\Omega_z = [-\frac{h}{2}, \frac{h}{2}]$ in a Cartesian coordinate (x,y,z). The plate is defined by an arbitrary region Ω in the (x,y) plane, located at the midplane for $z = 0$, and by a constant thickness h. See Fig. 1.

2.1.1. Constitutive relation

The plate can be made of NC perfectly bonded orthotropic layers. Using matrix notation, the three dimensional constitutive law of the kth layer is given by:

$$\begin{bmatrix} \sigma_{11}^{(k)} \\ \sigma_{22}^{(k)} \\ \sigma_{33}^{(k)} \\ \sigma_{23}^{(k)} \\ \sigma_{13}^{(k)} \\ \sigma_{12}^{(k)} \end{bmatrix} = \begin{bmatrix} C_{11}^{(k)} & C_{12}^{(k)} & C_{13}^{(k)} & 0 & 0 & C_{16}^{(k)} \\ & C_{22}^{(k)} & C_{23}^{(k)} & 0 & 0 & C_{26}^{(k)} \\ & & C_{33}^{(k)} & 0 & 0 & C_{36}^{(k)} \\ & & & C_{44}^{(k)} & C_{45}^{(k)} & 0 \\ & sym & & & C_{55}^{(k)} & 0 \\ & & & & & C_{66}^{(k)} \end{bmatrix} \begin{bmatrix} \varepsilon_{11}^{(k)} \\ \varepsilon_{22}^{(k)} \\ \varepsilon_{33}^{(k)} \\ \gamma_{23}^{(k)} \\ \gamma_{13}^{(k)} \\ \gamma_{12}^{(k)} \end{bmatrix} \quad \text{i.e. } [\sigma^{(k)}] = [C^{(k)}][\varepsilon^{(k)}] \tag{1}$$

where we denote the stress vector $[\sigma]$, the strain vector $[\varepsilon]$ and $C_{ij}^{(k)}$ the three-dimensional stiffness coefficients of the layer (k).

2.1.2. The weak form of the boundary value problem

Using the above matrix notation and for admissible displacement $\delta\vec{u} \in \delta U$, the variational principle is given by:

find $\vec{u} \in U$ (space of admissible displacements) such that

$$-\int_{\mathcal{V}} [\varepsilon(\delta\vec{u})]^T [\sigma(\vec{u})] d\mathcal{V} + \int_{\mathcal{V}} [\delta u]^T [b] d\mathcal{V} + \int_{\partial\mathcal{V}_F} [\delta u]^T [t] d\partial\mathcal{V} = 0, \quad \forall \delta\vec{u} \in \delta U \tag{2}$$

where $[b]$ and $[t]$ are the prescribed body and surface forces applied on $\partial\mathcal{V}_F$.

3. Application of the Proper Generalized Decomposition to plate

In this section, we briefly introduce the application of the PGD for plate analysis. This work is an extension of the previous studies on beam structures (Vidal et al., 2012a,b).

3.1. The displacement and the strain field

The displacement solution $(u_1(x,y,z), u_2(x,y,z), u_3(x,y,z))$ is constructed as the sum of N products of functions of in-plane coordinates and transverse coordinate ($N \in \mathbb{N}$ is the order of the representation)

$$[u] = \begin{bmatrix} u_1(x,y,z) \\ u_2(x,y,z) \\ u_3(x,y,z) \end{bmatrix} = \sum_{i=1}^{N} \begin{bmatrix} f_1^i(z)\, v_1^i(x,y) \\ f_2^i(z)\, v_2^i(x,y) \\ f_3^i(z)\, v_3^i(x,y) \end{bmatrix} \tag{3}$$

where (f_1^i, f_2^i, f_3^i) are defined in Ω_z and (v_1^i, v_2^i, v_3^i) are defined in Ω. In this paper, a classical eight-node FE approximation is used in Ω and a LW description is chosen in Ω_z as it is particulary suitable for the modeling of composite structure. The strain derived from Eq. (3) is

$$[\varepsilon(u)] = \sum_{i=1}^{N} \begin{bmatrix} f_1^i\, v_{1,1}^i \\ f_2^i\, v_{2,2}^i \\ (f_3^i)'\, v_3^i \\ (f_2^i)'\, v_2^i + f_3^i\, v_{3,2}^i \\ (f_1^i)'\, v_1^i + f_3^i\, v_{3,1}^i \\ f_1^i\, v_{1,2}^i + f_2^i\, v_{2,1}^i \end{bmatrix} \tag{4}$$

where the prime stands for the classical derivative $\left(f_i' = \frac{df_i}{dz}\right)$, and $()_{,\alpha}$ for the partial derivative.

3.2. The problem to be solved

For sake of clarity, the surfaces forces are neglected in the developments and the weak form of the plate problem introduced in Eq. (2) simplifies in

$$\int_{\Omega}\int_{\Omega_z}\left([\varepsilon(\delta\vec{u})]^T[C][\varepsilon(\vec{u})]+[\delta u]^T[b]\right)dz\,d\Omega=0 \tag{5}$$

where $[C]$ represents, in each layer (k), the matrix of the elastic moduli.

Eq. (5) is solved by an iterative procedure. If we assume that the first n functions have been already computed, the trial function for the iteration $n+1$ is written as

$$[u^{n+1}]=[u^n]+\begin{bmatrix} f_1\,v_1\\ f_2\,v_2\\ f_3\,v_3\end{bmatrix} \tag{6}$$

where (v_1,v_2,v_3), (f_1,f_2,f_3) are the functions to be computed and $[u^n]$ is the associated known set at iteration n defined by

$$[u^n]=\sum_{i=1}^{n}\begin{bmatrix} f_1^i\,v_1^i\\ f_2^i\,v_2^i\\ f_3^i\,v_3^i\end{bmatrix} \tag{7}$$

The test function is

$$\delta\begin{bmatrix} f_1\,v_1\\ f_2\,v_2\\ f_3\,v_3\end{bmatrix}=\begin{bmatrix} \delta f_1\,v_1+f_1\,\delta v_1\\ \delta f_2\,v_2+f_2\,\delta v_2\\ \delta f_3\,v_3+f_3\,\delta v_3\end{bmatrix}=[V]\,[\delta f]+[F]\,[\delta v] \tag{8}$$

with

$$[v]=\begin{bmatrix} v_1\\ v_2\\ v_3\end{bmatrix}\quad [f]=\begin{bmatrix} f_1\\ f_2\\ f_3\end{bmatrix}\quad [V]=\begin{bmatrix} v_1 & 0 & 0\\ 0 & v_2 & 0\\ 0 & 0 & v_3\end{bmatrix}\quad [F]=\begin{bmatrix} f_1 & 0 & 0\\ 0 & f_2 & 0\\ 0 & 0 & f_3\end{bmatrix} \tag{9}$$

The test function defined by Eq. (8) and the trial function defined by Eq. (6) are introduced into the weak form Eq. (5) to obtain the two following equations:

$$\begin{aligned}&\int_{\Omega}\int_{\Omega_z}\left([\varepsilon(F\,\delta v)]^T[C][\varepsilon(F v)]\right)dz\,d\Omega\\ &\quad=\int_{\Omega}\int_{\Omega_z}\left([F\,\delta v]^T[b]-[\varepsilon(F\,\delta v)]^T[C][\varepsilon(u^n)]\right)dz\,d\Omega\end{aligned} \tag{10}$$

$$\begin{aligned}&\int_{\Omega_z}\int_{\Omega}\left([\varepsilon(V\,\delta f)]^T[C][\varepsilon(Vf)]\right)d\Omega\,dz\\ &\quad=\int_{\Omega_z}\int_{\Omega}\left(-[\varepsilon(V\,\delta f)]^T[C][\varepsilon(u^n)]+[V\,\delta f]^T[b]\right)d\Omega\,dz\end{aligned} \tag{11}$$

As these equations define a coupled non linear problem, a non linear resolution strategy has to be used. The simplest strategy is a fixed point method. An initial function $f^{(0)}$ is set, and at each step, the algorithm computes a new pair $(v^{(m+1)},f^{(m+1)})$ such that

- $v^{(m+1)}$ satisfies Eq. (10) for f set to $f^{(m)}$ (i.e. F is given),
- $f^{(m+1)}$ satisfies Eq. (11) for v set to $v^{(m+1)}$ (i.e. V is given).

These two equations are linear and the first one is solved on Ω, while the second one is solved on Ω_z. The fixed point algorithm is stopped when

$$\frac{\|v^{(m+1)}f^{(m+1)}-v^{(m)}f^{(m)}\|_{\mathcal{V}}}{\|v^{(0)}f^{(0)}\|_{\mathcal{V}}}\leqslant\varepsilon \tag{12}$$

where $\|A\|_{\mathcal{V}}=\left[\int_{\Omega}\int_{\Omega_z}\sum_{i=1}^{3}A_i^2\,dx\,dy\,dz\right]^{1/2}$ and ε is a small parameter to be fixed by the user.

3.3. Finite element discretization

To build the plate finite element approximation, a discrete representation of the functions (v,f) must be introduced. We use a classical finite element approximation in Ω, and a polynomial expansion in Ω_z. The elementary vector of degrees of freedom (dof) associated with one element Ω_e of the mesh in Ω is denoted $[q_e^v]$. The vector of dofs associated with the polynomial expansion in Ω_z is denoted $[q^f]$. The displacement fields and the strain fields are determined from the values of $[q_e^v]$ and $[q^f]$ by

$$[v_e]=[N_{xy}][q_e^v],\quad [\mathcal{E}_v^e]=[B_{xy}][q_e^v],\quad [f]=[N_z][q^f]\ \text{ and }\ [\mathcal{E}_f]=[B_z][q^f] \tag{13}$$

where

$$[\mathcal{E}_v^e]^T=[\,v_1\quad v_{1,1}\quad v_{1,2}\quad v_2\quad v_{2,1}\quad v_{2,2}\quad v_3\quad v_{3,1}\quad v_{3,2}\,]$$

and

$$[\mathcal{E}_f]^T=[\,f_1\quad f_1'\quad f_2\quad f_2'\quad f_3\quad f_3'\,]$$

The matrices $[N_{xy}]$, $[B_{xy}]$, $[N_z]$, $[B_z]$ contain the interpolation functions, their derivatives and the jacobian components.

3.4. Finite element problem to be solved on Ω

For the sake of simplicity, the function $f^{(m)}$ which is assumed to be known, will be denoted $\tilde{f}$ (and $\tilde{F}$), and the function $v^{(m+1)}$ to be computed will be denoted v. The strain in Eq. (10) is defined in matrix notations as

$$[\varepsilon(\tilde{F}\,v)]=[\Sigma_z(\tilde{f})][\mathcal{E}_v] \tag{14}$$

with

$$[\Sigma_z(\tilde{f})]=\begin{bmatrix} 0 & \tilde{f}_1 & 0 & 0 & 0 & 0 & 0 & 0 & 0\\ 0 & 0 & 0 & 0 & 0 & \tilde{f}_2 & 0 & 0 & 0\\ 0 & 0 & 0 & 0 & 0 & 0 & \tilde{f}_3' & 0 & 0\\ 0 & 0 & 0 & \tilde{f}_2' & 0 & 0 & 0 & 0 & \tilde{f}_3\\ \tilde{f}_1' & 0 & 0 & 0 & 0 & 0 & 0 & \tilde{f}_3 & 0\\ 0 & 0 & \tilde{f}_1 & 0 & \tilde{f}_2 & 0 & 0 & 0 & 0\end{bmatrix} \tag{15}$$

The variational problem defined on Ω from Eq. (10) is

$$\begin{aligned}\int_{\Omega}[\delta\mathcal{E}_v]^T[k_z(\tilde{f})][\mathcal{E}_v]d\Omega=&\int_{\Omega}[\delta v]^T[b_z(\tilde{f})]d\Omega\\ &-\int_{\Omega}[\delta\mathcal{E}_v]^T[\sigma_z(\tilde{f},u^n)]d\Omega\end{aligned} \tag{16}$$

with

$$[k_z(\tilde{f})]=\int_{\Omega_z}[\Sigma_z(\tilde{f})]^T[C][\Sigma_z(\tilde{f})]dz \tag{17}$$

$$[b_z(\tilde{f})]=\int_{\Omega_z}\left[\tilde{F}\right]^T[b]dz \tag{18}$$

$$[\sigma_z(\tilde{f},u^n)]=\int_{\Omega_z}[\Sigma_z(\tilde{f})]^T[C][\varepsilon(u^n)]dz \tag{19}$$

The introduction of the finite element approximation Eq. (13) in the variational Eq. (16) leads to the linear system

$$\left[K_z(\tilde{f})\right][q^v]=\left[\mathcal{R}_v(\tilde{f},u^n)\right] \tag{20}$$

where

- $[q^v]$ is the vector of the nodal displacements associated with the finite element mesh in Ω,

- $\left[K_z(\tilde{f})\right]$ is the stiffness matrix obtained by summing the elements' stiffness matrices $\left[K_z^e(\tilde{f})\right] = \int_{\Omega_e}[B_{xy}]^T[k_z(\tilde{f})][B_{xy}]d\Omega_e$,
- $\left[\mathcal{R}_v(\tilde{f},u^n)\right]$ is the equilibrium residual obtained by summing the elements' residual load vectors $\left[\mathcal{R}_v^e(\tilde{f},u^n)\right] = \int_{\Omega_e}[N_{xy}]^T[b_z(\tilde{f})]dx - \int_{\Omega_e}[B_{xy}]^T[\sigma_z(\tilde{f},u^n)]d\Omega_e$.

3.5. Finite element problem to be solved on Ω_z

For the sake of simplicity, the function $v^{(m+1)}$ which is assumed to be known, will be denoted $\tilde{v}$ (and $\tilde{V}$), and the function $f^{(m+1)}$ to be computed will be denoted f. The strain in Eq. (11) is defined in matrix notations as

$$[\varepsilon(\tilde{V}f)] = [\Sigma_{xy}(\tilde{v})][\mathcal{E}_f] \tag{21}$$

with

$$[\Sigma_{xy}(\tilde{v})] = \begin{bmatrix} \tilde{v}_{1,1} & 0 & 0 & 0 & 0 & 0 \\ 0 & 0 & \tilde{v}_{2,2} & 0 & 0 & 0 \\ 0 & 0 & 0 & 0 & 0 & \tilde{v}_3 \\ 0 & 0 & 0 & \tilde{v}_2 & \tilde{v}_{3,2} & 0 \\ 0 & \tilde{v}_1 & 0 & 0 & \tilde{v}_{3,1} & 0 \\ \tilde{v}_{1,2} & 0 & \tilde{v}_{2,1} & 0 & 0 & 0 \end{bmatrix} \tag{22}$$

The variational problem defined on Ω_z from Eq. (11) is

$$\int_{\Omega_z}[\delta\mathcal{E}_f]^T[k_{xy}(\tilde{v})][\mathcal{E}_f]dz = \int_{\Omega_z}[\delta F]^T[b_{xy}(\tilde{v})]dz - \int_{\Omega_z}[\delta\mathcal{E}_f]^T[\sigma_{xy}(\tilde{v},u^n)]dz \tag{23}$$

with

$$[k_{xy}(\tilde{v})] = \int_\Omega[\Sigma_{xy}(\tilde{v})]^T[C][\Sigma_{xy}(\tilde{v})]d\Omega \tag{24}$$

$$[b_{xy}(\tilde{v})] = \int_\Omega\left[\tilde{V}\right]^T[b]d\Omega \tag{25}$$

$$[\sigma_{xy}(\tilde{v},u^n)] = \int_\Omega[\Sigma_{xy}(\tilde{v})]^T[C][\varepsilon(u^n)]d\Omega \tag{26}$$

The introduction of the finite element discretization Eq. (13) in the variational Eq. (23) leads to the linear system

$$\left[K_{xy}(\tilde{v})\right]\left[q^f\right] = \left[\mathcal{R}_f(\tilde{v},u^n)\right] \tag{27}$$

where $\left[q^f\right]$is the vector of degree of freedom associated with the polynomial expansion in Ω_z, $\left[K_{xy}(\tilde{v})\right]$ is a stiffness matrix defined by Eq. (28) and $\left[\mathcal{R}_f(\tilde{v},u^n)\right]$ an equilibrium residual defined by Eq. (29)

$$\left[K_{xy}(\tilde{v})\right] = \int_{\Omega_z}[B_z]^T[k_{xy}(\tilde{v})][B_z]dz \tag{28}$$

$$\left[\mathcal{R}_f(\tilde{v},u^n)\right] = \int_{\Omega_z}[N_z]^T[b_{xy}(\tilde{v})]dz - \int_{\Omega_z}[B_z]^T[\sigma_{xy}(\tilde{v},u^n)]dz \tag{29}$$

Remark. To take into account the surface loads in Eqs. (16)–(19) and (23)–(26), it is needed to replace $[b]$ by $[t\ \delta(z\pm\frac{h}{2})]$.

4. Numerical results

In this section, an eight-node quadrilateral FE based on the classical Serendipity interpolation functions is used for the unknowns depending on the in-plane coordinates. A Gaussian numerical integration with 3×3 points is used to evaluate the elementary matrices. As far as the integration with respect to the transverse coordinate is concerned, an analytical integration is performed. Several static tests are presented validating our approach and evaluating its efficiency.

First, a comparison between the first-order (Bognet et al., 2012) and the fourth-order z-expansion is performed upon a simple homogeneous plate. This study aims at highlighting the more suitable approach to compute local and global quantities for plate structures. It concerns both the choice of the degree of the z-expansion and the required type of mesh. Then, the capability of the more accurate and efficient approach, i.e. that associated to the fourth-order expansion, is shown on symmetric, anti-symmetric laminates and sandwich plates for very thick to thin case. The influence of the boundary conditions is also addressed: a global and localized pressure are considered. The results are compared with the exact elasticity solution (Pagano, 1970). It is important to note that the transverse shear and normal stresses are computed directly by the Hooke's law.

In the following, the plate is discretized with $N_x\times N_y$ elements. The total number of numerical layer is denoted N_z. The numbers of dofs are also precised for the two problems associated to v_j^i and f_j^i. They are denoted $Ndof_{xy}$ and $Ndof_z$ respectively. Notice that the convergence velocity of the fixed point process (cf. Section 3.2) is high. Usually, only a maximum of three iterations is required to reach the convergence as in Nouy (2010).

4.1. Influence of the degree of the z-expansion

A comparison based on global and local mechanical quantities between two different orders of z-expansion is carried out. The first one is the first-order approach (denoted $d^\circ1$) developed in Bognet et al. (2012) and the present one involves a fourth-order approach (denoted $d^\circ4$). For this purpose, the test case concerns an homogeneous plate to assess the relevance of this expansion. The following data are considered:

geometry: square plate of length $a=b=0.1$ and length-to-thickness ratio $S=\frac{a}{h}=10$ and $S=2,100$;
boundary conditions: simply supported on all sides, bi-sinusoidal transverse distributed load on the top surface $p_3(x_1,x_2,z=\frac{h}{2})=p_0\ \sin\frac{\pi x_1}{a}\ \sin\frac{\pi x_2}{b}$;
materials: isotropic material with $E=73$ GPa and $v=0.34$;
mesh: regular meshes $N_x=N_y=1,2,4,8,16,32$ and refined meshes with space ratio, denoted sr(x), are used for the quarter of the plate. x is the ratio between the size of the larger and the smaller element. The mesh is refined near the edges;
order of z-expansion, numerical layers: $N_z=4$ with $d^\circ1$, $N_z=1$ with $d^\circ4$
results: displacements and stresses are made non-dimensional according to $\bar{u}_3=u_3(a/2,b/2,h/2)\frac{100Eh^3}{p_0a^4}$; $\bar{\sigma}_{11}=\sigma_{11}(a/2,b/2,h/2)\frac{1}{p_0S^2}$; $\bar{\sigma}_{13}=\sigma_{13}(0,b/2,0)\frac{1}{p_0S}$; $\bar{\sigma}_{33}=\sigma_{33}(a/2,b/2,h/2)\frac{1}{p_0}$;
reference values: the three-dimensional exact elasticity results are obtained as in Demasi (2008).

Four numerical layers for $d^\circ1$ are chosen so as to have the same number of dofs in the two tests. In each case, only one couple is built. First, a convergence study is addressed for the length-to-thickness ratio $S=10$. The results are given in Fig. 2 for the strain energy, $\bar{u}_3$, $\bar{\sigma}_{11}$, $\bar{\sigma}_{13}$ and $\bar{\sigma}_{33}$. The convergence rate is the same for the two orders of z-expansion, but the accuracy is rather different. The error rate for the strain energy and the deflection is about 2% for the $d^\circ1$ approach, while the $d^\circ4$ expansion gives the reference solution. From a local point of view, the fourth-order expansion drives to an error rate of less than 1.2% with a $N_x=N_y=16$ mesh. Concerning the first-order approach, the error is around 10% for $\bar{\sigma}_{11}$, 6% for $\bar{\sigma}_{13}$ and 500% for $\bar{\sigma}_{33}$.

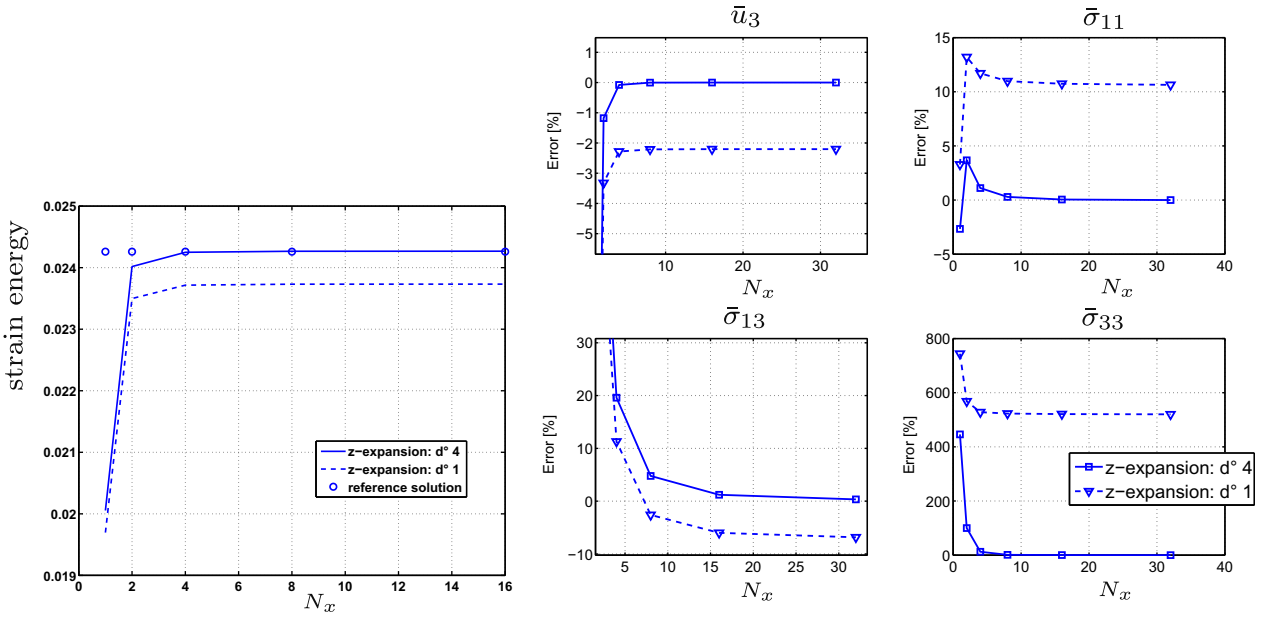

Fig. 2. Convergence study with respect to $N_x = N_y$ of the strain energy (left), $\bar{u}_3$, $\bar{\sigma}_{11}$, $\bar{\sigma}_{13}$ and $\bar{\sigma}_{33}$ (right) – $S = 10$ – isotropic plate – $b = a$ – $N_z = 4$ with $d^\circ 1$, $N_z = 1$ with $d^\circ 4$.

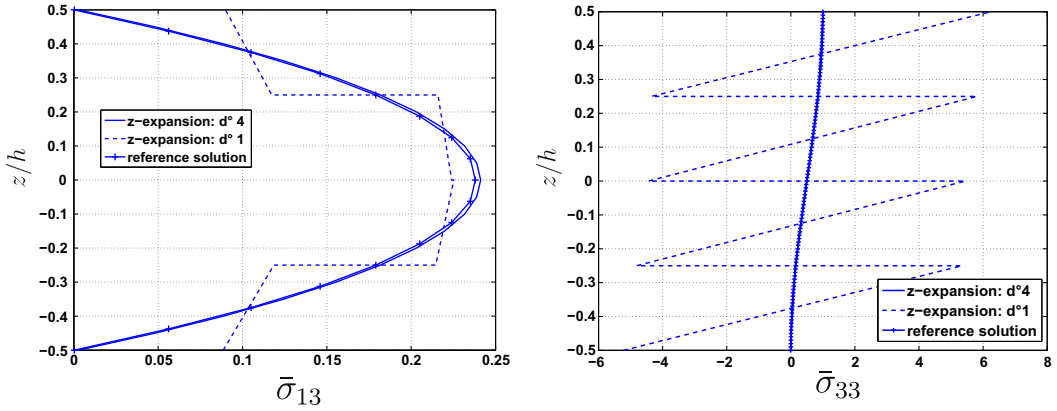

Fig. 3. Distribution of $\bar{\sigma}_{13}$ (left) and $\bar{\sigma}_{33}$ (right) along the thickness – $S = 10$ – isotropic plate – $b = a$ – $N_z = 4$ with $d^\circ 1$, $N_z = 1$ with $d^\circ 4$.

For further comparison, the distribution of the transverse shear and normal stresses are shown in Fig. 3 with a converged mesh. We note that the results with the fourth-order z-expansion are in excellent agreement with the reference solution. We can also deduce that the number of numerical layers in the first-order approach is insufficient. Strong discontinuities appear in the through-thickness distributions. Moreover, oscillations occur for the transverse normal stress. The prescribed boundary conditions on the top and bottom surfaces are not fulfilled.

To improve the results of the first-order z-expansion, the influence of the numerical layers is addressed. The convergence study is presented in Fig. 4 for $N_z = 4$ to $N_z = 32$. The strain energy is very close to the reference solution. For the local quantities, the error rate of the in-plane and transverse shear stresses becomes less than 2% for $N_z \geqslant 32$. Nevertheless, the convergence rate for the transverse normal stress is rather slow and discontinuities remain. A much more important refinement in the z-direction is required to achieve converged results.

In conclusion, with respect to the number of dofs, the fourth-order z-expansion approach is more efficient to recover local quantities and accurate through-the-thickness distributions. Only the results associated with this present expansion are presented in the following tests.

4.2. Influence of the mesh

For very thick ($S = 2$) and very thin ($S = 100$) plates as described in the previous section, the influence of the mesh on the accuracy of the local results is evaluated. The distributions of the deflection, in-plane and transverse shear stresses along the thickness are shown in Figs. 5 and 6 for the two slenderness ratios. A convergence study is carried out using different number of elements with a constant value of space ratio. A regular mesh with $N_x = N_y = 16$ is also considered. For all the results, we check that the convergence values are very close to the reference solution (error rate of less than 1%). It is inferred from Fig. 5 (thick case) that the considered meshes have no influence on the results. Concerning the thin case, it should be noted that the convergence rate is very quick for the out-of-plane displacement and the in-plane stress. On the contrary, the transverse shear stress (Fig. 6 right) is very sensitive to the mesh. The $N_x = N_y = 16$ mesh with sr(20) is needed to recover reference distributions. For thin structure, a refinement of the mesh is unavoidable to find accu-

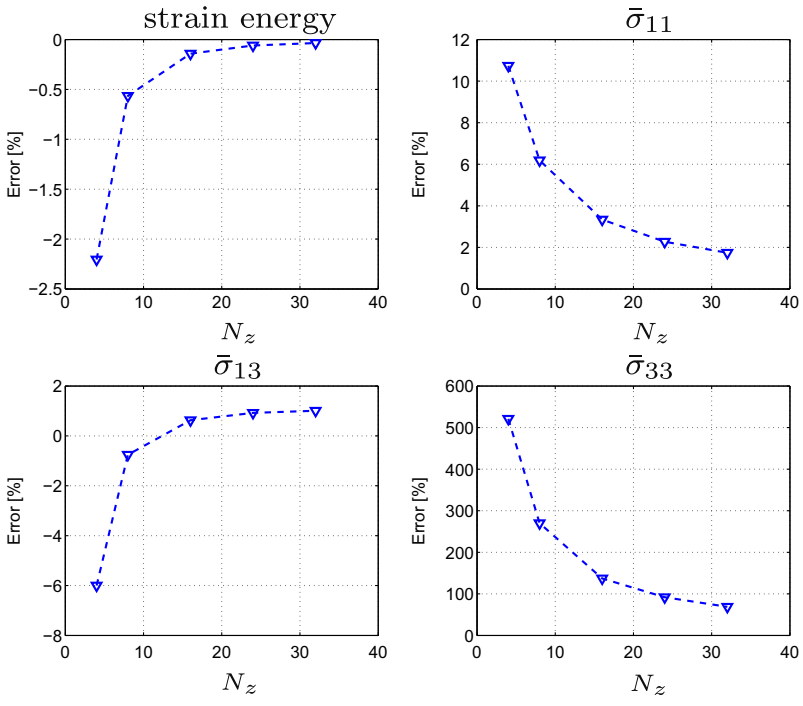

Fig. 4. Convergence study with respect to N_z of the strain energy, $\bar{\sigma}_{11}$, $\bar{\sigma}_{13}$ and $\bar{\sigma}_{33}$ (right) – $S = 10$ – isotropic plate – $b = a$ – $d^{\circ}1$.

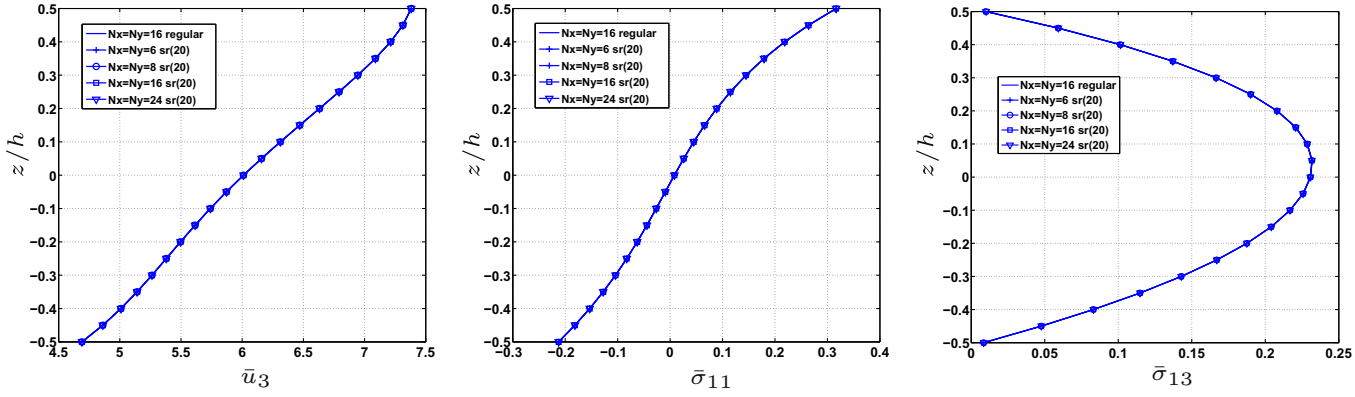

Fig. 5. Convergence study on the distribution of $\bar{u}_3$ (left), $\bar{\sigma}_{11}$ (middle) and $\bar{\sigma}_{13}$ (right) along the thickness – $S = 2$ – isotropic plate – $b = a$ – $d^{\circ}4$.

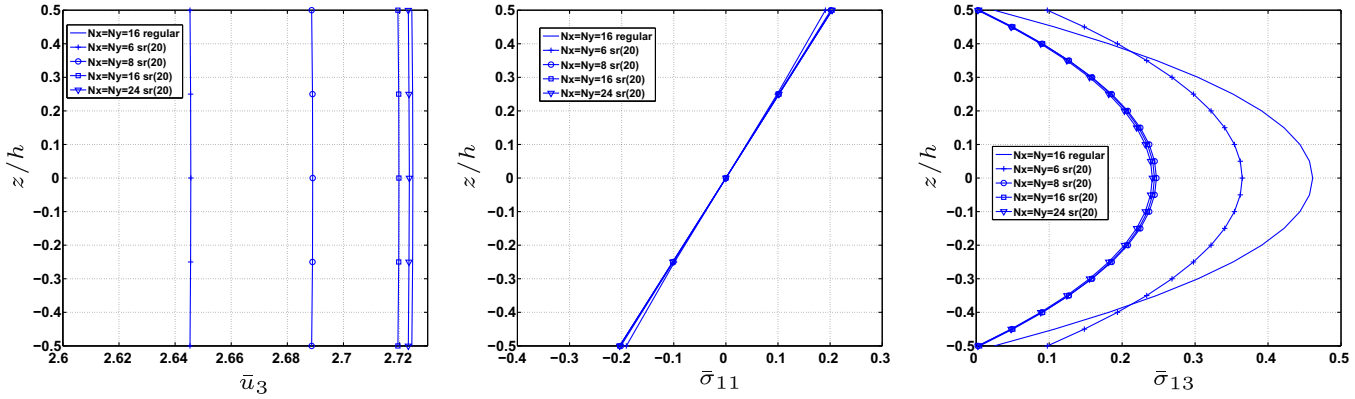

Fig. 6. Convergence study on the distribution of $\bar{u}_3$ (left), $\bar{\sigma}_{11}$ (middle) and $\bar{\sigma}_{13}$ (right) along the thickness – $S = 100$ – isotropic plate – $b = a$ – d°4.

Table 1
Four layers $(0^\circ/90^\circ/0^\circ/90^\circ)$ – $b = 3a$ – $N_x = N_y = 16$ sr(12) – $N_z = NC$.

S	Model	$\bar{u}(h/2)$	$\bar{v}(-h/2)$	$\bar{w}(0)$	$\bar{\sigma}_{11}(-h/2)$	$\bar{\sigma}_{22}(h/2)$	$\bar{\sigma}_{12}(h/2)$	$\bar{\sigma}_{13}(0)$	$\bar{\sigma}_{23}(0)$	$\bar{\sigma}_{33}(0)$
2	Present	−0.0848	0.0356	10.5470	−2.0498	0.6419	−0.0742	0.3290	0.1056	0.5484
	Error	0.00%	0.00%	0.00%	0.00%	0.01%	0.00%	0.00%	0.08%	0.00%
	Exact	−0.0848	0.0356	10.5472	−2.0497	0.6419	−0.0742	0.3290	0.1055	0.5483
4	Present	−0.0438	0.0199	3.9272	−1.4537	0.3400	−0.0400	0.4549	0.0790	0.6345
	Error	0.00%	0.00%	0.00%	0.00%	0.00%	0.00%	0.00%	0.03%	0.00%
	Exact	−0.0438	0.0199	3.9271	−1.4536	0.3400	−0.0400	0.4549	0.0790	0.6345
10	Present	−0.0254	0.0099	1.5891	−1.1156	0.1741	−0.0223	0.5333	0.0480	0.6834
	Error	0.00%	0.00%	0.00%	0.00%	0.01%	0.01%	0.01%	0.06%	0.00%
	Exact	−0.0254	0.0099	1.5891	−1.1156	0.1740	−0.0223	0.5333	0.0480	0.6834
40	Present	−0.0213	0.0073	1.1171	−1.0386	0.1301	−0.0179	0.5529	0.0388	0.6993
	Error	0.00%	0.03%	0.01%	0.00%	0.09%	0.04%	0.07%	0.77%	0.57%
	Exact	−0.0213	0.0073	1.1173	−1.0386	0.1299	−0.0179	0.5525	0.0385	0.6954
100	Present	−0.0210	0.0072	1.0895	−1.0341	0.1275	−0.0177	0.5564	0.0398	0.7524
	Error	0.00%	0.03%	0.06%	0.00%	0.18%	0.10%	0.48%	4.97%	8.09%
	Exact	−0.0210	0.0072	1.0902	−1.0341	0.1273	−0.0176	0.5537	0.0379	0.6961

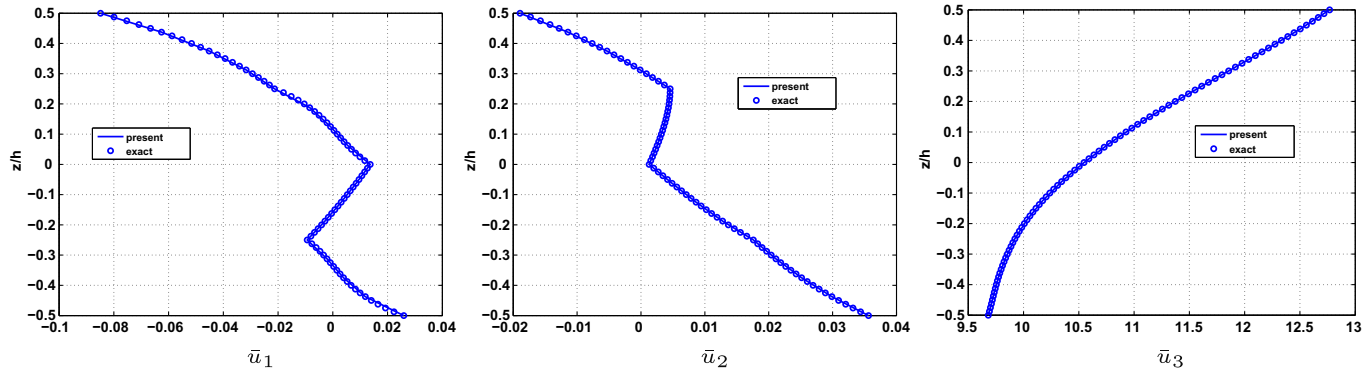

Fig. 7. Distribution of $\bar{u}_1$ (left), $\bar{u}_2$ (middle) and $\bar{u}_3$ (right) along the thickness – $S = 2$–4 layers – $b = 3a$ – $d°4$.

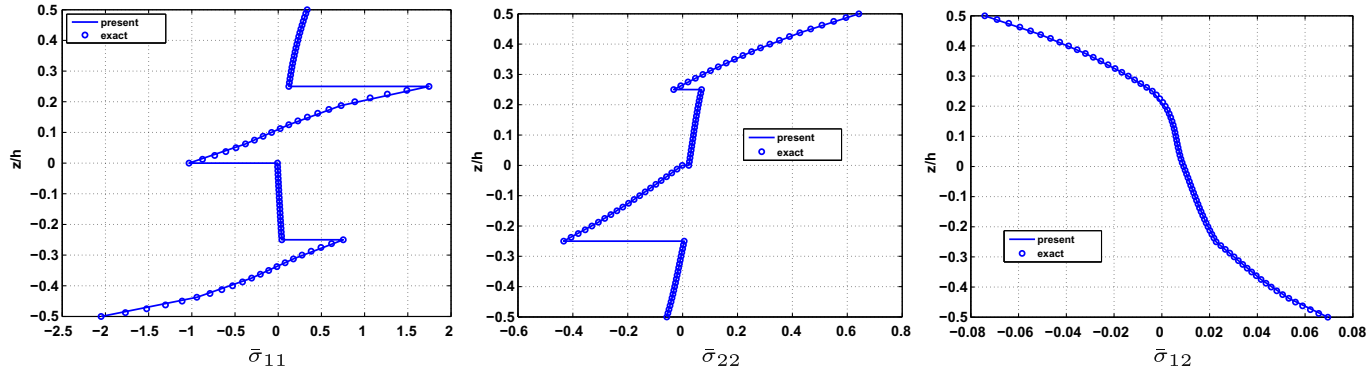

Fig. 8. Distribution of $\bar{\sigma}_{11}$ (left), $\bar{\sigma}_{22}$ (middle) and $\bar{\sigma}_{12}$ (right) along the thickness – $S = 2$–4 layers – $b = 3a$ – $d°4$.

rate transverse shear stresses. This type of mesh is used in the following composite tests.

4.3. bending analysis of anti-symmetric plate under bi-sinusoidal pressure

A simply-supported plate submitted to a bi-sinusoidal pressure is considered. The test is described below:

geometry: rectangular composite cross-ply plate $(0^\circ/90^\circ/0^\circ/90^\circ)$ with $b = 3a$. All layers have the same thickness. $S = \frac{a}{h} \in \{2, 4, 10, 40, 100\}$;
boundary conditions: simply-supported plate on all sides subjected to a bi-sinusoidal pressure $q(x, y) = q_0 \sin\frac{\pi x}{a} \sin\frac{\pi y}{b}$;
material properties: $E_L = 25$ GPa, $E_T = 1$ GPa, $G_{LT} = 0.2$ GPa, $G_{TT} = 0.5$ GPa, $\nu_{LT} = \nu_{TT} = 0.25$
where L refers to the fiber direction, T refers to the transverse direction;
mesh: $N_x = N_y = 16$ with a space ratio of 12 (denoted sr(12)). Only one quarter of the plate is meshed;
number of dofs: $Ndof_{xy} = 2499$ and $Ndof_z = 12 \times NC + 3 = 51$;
results: the results are made nondimensional using:

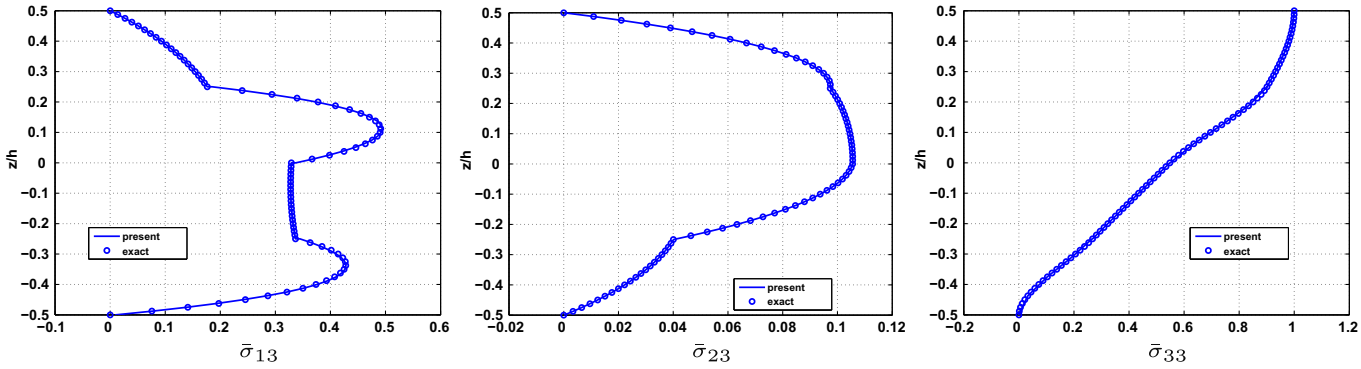

Fig. 9. Distribution of $\bar{\sigma}_{13}$ (left), $\bar{\sigma}_{23}$ (middle) and $\bar{\sigma}_{33}$ (right) along the thickness – $S = 2$–4 layers – $b = 3a$ – $d°4$.

$$\bar{u} = u_1(0, b/2, z)\frac{E_T}{hq_0S^3}, \quad \bar{v} = u_2(a/2, 0, z)\frac{E_T}{hq_0S^3},$$
$$\bar{w} = u_3(a/2, b/2, z)\frac{100E_T}{S^4hq_0}$$

$$\bar{\sigma}_{\alpha\alpha} = \frac{\sigma_{\alpha\alpha}(a/2, b/2, z)}{q_0S^2}, \quad \bar{\sigma}_{12} = \frac{\sigma_{12}(0, 0, z)}{q_0S^2}$$

$$\bar{\sigma}_{13} = \frac{\sigma_{13}(0, b/2, z)}{q_0S}, \quad \bar{\sigma}_{23} = \frac{\sigma_{23}(a/2, 0, z)}{q_0S},$$
$$\bar{\sigma}_{33} = \frac{\sigma_{33}(a/2, b/2, z)}{q_0}$$

reference values: the three-dimensional exact elasticity results are obtained as in Pagano (1970).

The performance of the approach is illustrated for very thick to thin plates. The small value of the slenderness ratio aims at showing the range of validity of the method. Here, only one couple is needed in the PGD expansion Eq. (3), as the boundary conditions are not severe. It is inferred from Table 1 that the present results are in excellent agreement with the reference exact solution regardless of the value of S. The maximum error rate is 0.77%, except for the transverse shear stress with $S = 100$ (≈5%). A more refined mesh allows to decrease this error rate. For further comparison, the distribution of the displacements and stresses are given in Figs. 7–9. The zig-zag effect of the in-plane displacements is well-represented. The transverse displacement is not linear through the thickness. Note that the distribution of the in-plane stresses in Fig. 8 is not symmetric as expected. Finally, continuity conditions at the layer interfaces and the boundary conditions on the lower and upper surfaces for the transverse shear and normal stresses are nearly fullfilled, see Fig. 9.

4.4. Bending analysis of symmetric plate under localized pressure

In this section, we focus on the ability of the approach to capture local effects. This test is about simply-supported plate submitted to a localized pressure. It is shown in Fig. 10 and detailed below:

geometry: square composite cross-ply plate $(0°/90°/0°), a = b$. All layers have the same thickness. $S \in \{4, 10, 40, 100\}$;
boundary conditions: simply-supported plate subjected to a localized pressure $q(x, y) = q_0$ applied on a square area with a size of $a/10 \times b/10$ at the plate center (see Fig. 10 right);
material properties: same material as in Section 3.2;
mesh: $N_x = N_y = 22$ sr(14) (see Fig. 10 left), a quarter of the plate is meshed;

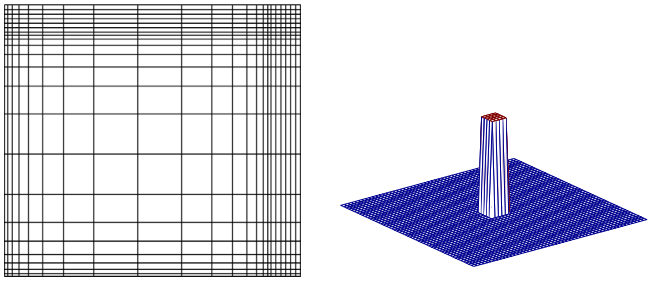

Fig. 10. Mesh $N_x = N_y = 22$ sr(14) (left) – localized pressure (right).

number of dofs: $Ndof_{xy} = 4623$ and $Ndof_z = 12 \times NC + 3 = 39$;
results: displacements and stresses are made non-dimensional as in Section 4.3;
reference values: they are obtained with 450 terms in the Fourier series (Pagano, 1970). The applied pressure is shown in Fig. 10 right.

The number of couples built by the present approach varies from five for $S = 100$ to twelve for $S = 4$. The number of couples increases with the thickness of the structure. As seen in Table 2, the results perform very well with respect to the reference solution. The maximum error rate remains less than 2.8%. The evolution of the displacements and stresses along the thickness are presented in Fig. 11–13. The previous comments are confirmed. We also notice that the in-plane stresses $\sigma_{\alpha\alpha}, \alpha = 1, 2$ are influenced by the localized pressure, especially in the upper layer. The evolution through the thickness becomes highly non-linear in this layer. Moreover, a strong non-symmetric distribution appears. This specific behavior is well-captured. For the transverse shear and normal stresses, the upper and lower conditions are satisfied. A small discontinuity for σ_{23} between two adjacent layers appears without affecting the accuracy of the method with respect to the reference solution.

4.5. Bending analysis of sandwich plate under bi-sinusoidal pressure

The approach is now assessed on a sandwich plate. The test is described as follows:

geometry: square sandwich plate with length-to-thickness ratios $S \in \{2, 4, 10, 40, 100\}$. The thickness of each face sheet is $\frac{h}{10}$.
boundary conditions: simply-supported plate subjected to bi-sinusoidal load

$$q(x, y) = q_0 \sin\frac{\pi x}{a} \sin\frac{\pi y}{b};$$

Table 2
Three layers $(0^\circ/90^\circ/0^\circ)$ – SS-localized pressure – $b = a$ – $N_x = N_y = 22$ sr(14) – $N_z = NC$.

S	Model	$\bar{u}(h/2) \times 10^{-4}$	$\bar{v}(-h/2) \times 10^{-4}$	$\bar{w}(0)$	$\bar{\sigma}_{11}(h/2)$	$\bar{\sigma}_{22}(-h/6)$	$\bar{\sigma}_{12}(h/2) \times 10^{-4}$	$\bar{\sigma}_{13}(0)$	$\bar{\sigma}_{23}(0)$	$\bar{\sigma}_{33}(0)$
4	Present	−3.76	7.86	0.1196	0.2563	−0.0512	−15.5	0.0089	0.0029	0.2067
	Error	0.2%	0.2%	0.2%	2.8%	2.6%	0.1%	0.0%	0.5%	0.92%
	Exact	−3.77	7.85	0.1198	0.2639	−0.0526	−15.6	0.0089	0.0029	0.2086
10	Present	−2.97	3.34	0.0420	0.0757	−0.0427	−8.54	0.0115	−0.0016	0.4564
	Error	0.2%	0.1%	0.2%	1.1%	0.3%	0.1%	0.3%	1.0%	1.03%
	Exact	−2.98	3.34	0.0421	0.0748	−0.0428	−8.55	0.0116	−0.0016	0.4611
40	Present	−2.91	1.89	0.0223	0.0425	−0.0327	−5.85	0.0112	−0.0022	0.5091
	Error	0.1%	0.0%	0.1%	1.0%	0.5%	0.0%	1.1%	0.9%	1.04%
	Exact	−2.90	1.89	0.0223	0.0429	−0.0325	−5.85	0.0111	−0.0023	0.5039
100	Present	−2.90	1.80	0.0210	0.0406	−0.0303	−5.65	0.0110	−0.0023	0.5028
	Error	0.0%	0.1%	0.0%	0.1%	0.0%	0.1%	0.3%	1.4%	0.56%
	Exact	−2.90	1.80	0.0210	0.0406	−0.0303	−5.65	0.0109	−0.0023	0.5000

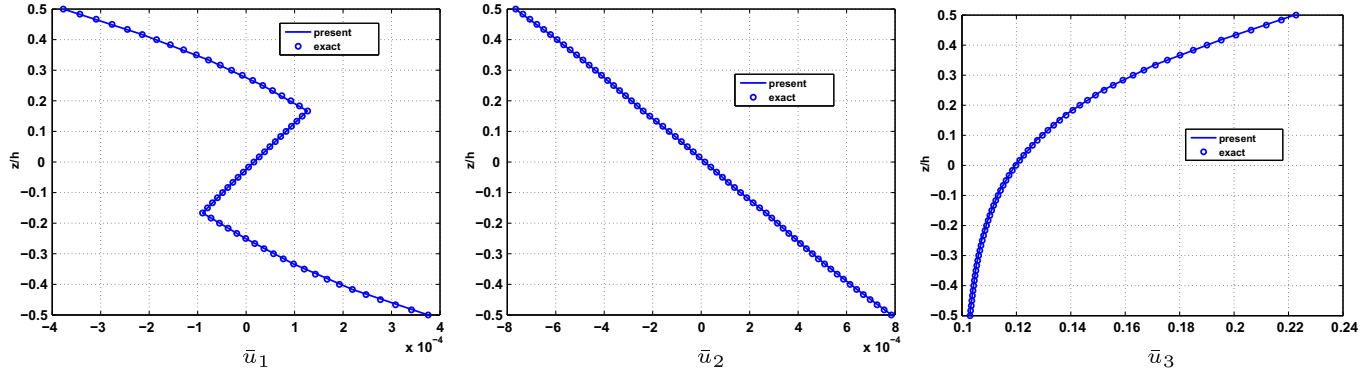

Fig. 11. Distribution of $\bar{u}_1$ (left), $\bar{u}_2$ (middle) and $\bar{u}_3$ (right) along the thickness – $S = 4$ – 3 layers – localized pressure – $d^\circ 4$.

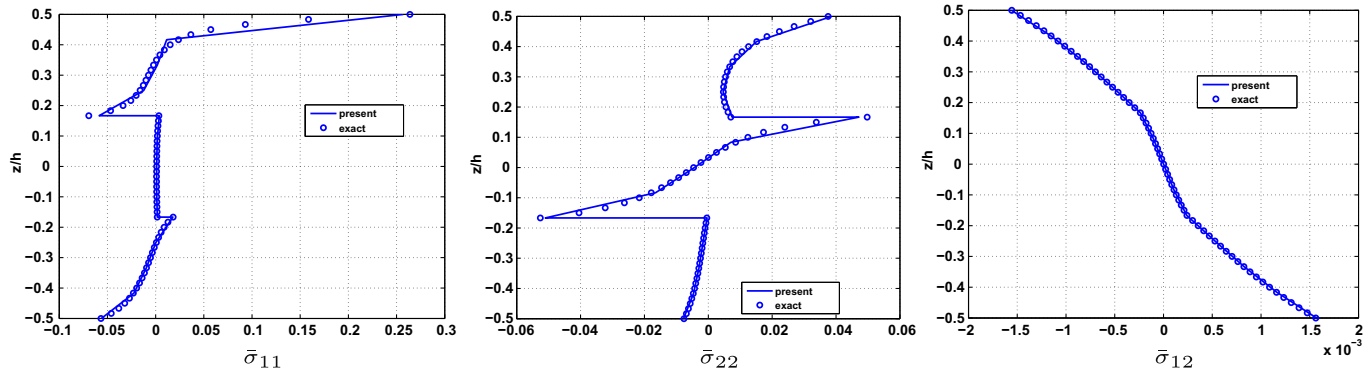

Fig. 12. Distribution of $\bar{\sigma}_{11}$ (left), $\bar{\sigma}_{22}$ (middle) and $\bar{\sigma}_{12}$ (right) along the thickness – $S = 4$ – 3 layers – localized pressure – $d^\circ 4$.

material properties: the material of the face sheet is the same as in Section 4.3.
The core material is transversely isotropic with respect to z and is characterized by:

$$E_{xx} = E_{yy} = 0.04\ \text{GPa}, \quad E_{zz} = 0.5\ \text{GPa}, \quad G_{xz} = G_{yz} = 0.06\ \text{GPa},$$
$$G_{xy} = 0.016\ \text{GPa}, \quad \nu_{xz} = \nu_{yz} = 0.02, \quad \nu_{xy} = 0.25$$

mesh: $N_x = N_y = 16$ sr(12) is used for the quarter of the plate;
number of dofs: $Ndof_{xy} = 2499$ and $Ndof_z = 12 \times NC + 3 = 39$;
results: displacements and stresses are made non-dimensional as in Section 4.3;
reference values: the three-dimensional exact elasticity results are obtained as in Pagano (1970).

Only one couple is needed for this configuration. The results are summarized in Table 3. The approach is also suitable to model very thick to thin sandwich structures with an error rate of less than 2.43%. Fig. 14 shows the in-plane and transverse displacements along the thickness. Figs. 15 and 16 present the distribution of the in-plane, transverse shear and normal stresses along the thickness. The results perform very well with respect to the reference solution. The non-linear variation of the displacement through the thickness is recovered and the high variation of the transverse

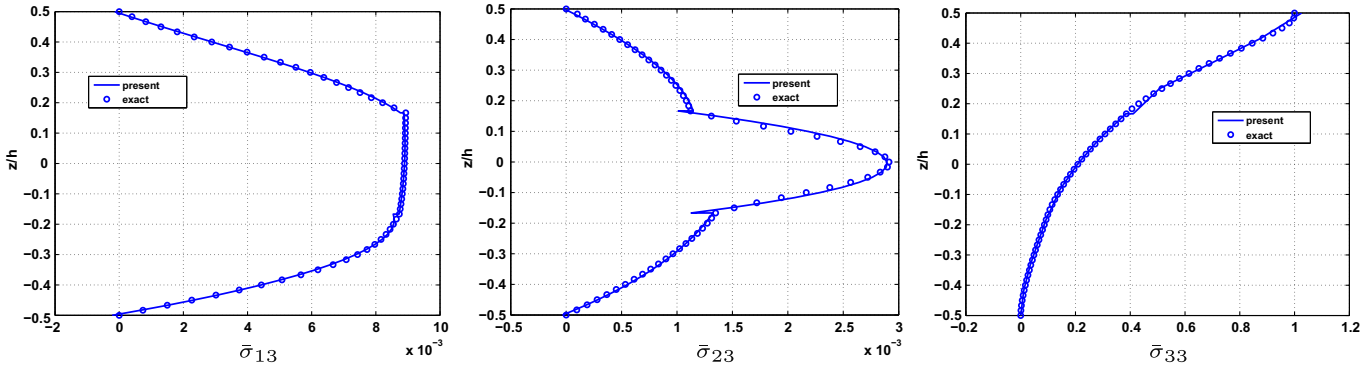

Fig. 13. Distribution of $\bar{\sigma}_{13}$ (left), $\bar{\sigma}_{23}$ (middle) and $\bar{\sigma}_{33}$ (right) along the thickness – $S = 4$–3 layers – localized pressure – $d^{\circ}4$.

Table 3
Sandwich plate – $b = a$ – $N_x = N_y = 16$ sr(12) – $N_z = NC$.

S	Model	$\bar{u}(h/2)$	$\bar{v}(-h/2)$	$\bar{w}(0)$	$\bar{\sigma}_{11}(h/2)$	$\bar{\sigma}_{22}(h/2)$	$\bar{\sigma}_{12}(h/2)$	$\bar{\sigma}_{13}(0)$	$\bar{\sigma}_{13}$ max	$\bar{\sigma}_{23}(0)$	$\bar{\sigma}_{33}(0)$
2	Present	−0.0395	0.1163	22.1025	3.2782	0.4517	−0.2403	0.1848	0.3204	0.1399	0.4918
	Error	0.00%	0.00%	0.00%	0.01%	0.00%	0.00%	0.02%	0.11%	0.03%	0.02%
	Exact	−0.0395	0.1163	22.1029	3.2781	0.4517	−0.2403	0.1848	0.3201	0.1399	0.4917
4	Present	−0.0188	0.0758	7.5963	1.5559	0.2595	−0.1437	0.2387	0.2387	0.1072	0.5002
	Error	0.00%	0.00%	0.00%	0.01%	0.00%	0.01%	0.01%	0.01%	0.01%	0.00%
	Exact	−0.0188	0.0758	7.5962	1.5558	0.2595	−0.1437	0.2387	0.2387	0.1072	0.5002
10	Present	−0.0143	0.0313	2.2004	1.1532	0.1105	−0.0707	0.2998	0.2998	0.0527	0.5001
	Error	0.00%	0.00%	0.00%	0.01%	0.01%	0.01%	0.01%	0.01%	0.03%	0.00%
	Exact	−0.0143	0.0313	2.2004	1.1531	0.1104	−0.0707	0.2998	0.2998	0.0527	0.5002
40	Present	−0.0138	0.0151	0.9665	1.1001	0.0584	−0.0453	0.3226	0.3226	0.0313	0.5000
	Error	0.00%	0.03%	0.01%	0.00%	0.05%	0.04%	0.02%	0.02%	0.32%	0.00%
	Exact	−0.0138	0.0151	0.9665	1.1001	0.0584	−0.0453	0.3225	0.3225	0.0312	0.5000
100	Present	−0.0138	0.0140	0.8921	1.0975	0.0550	−0.0437	0.3246	0.3266	0.0305	0.5000
	Error	0.00%	0.07%	0.03%	0.00%	0.14%	0.11%	0.20%	0.80%	2.43%	0.01%
	Exact	−0.0138	0.0140	0.8924	1.0975	0.0550	−0.0437	0.3240	0.3240	0.0297	0.5000

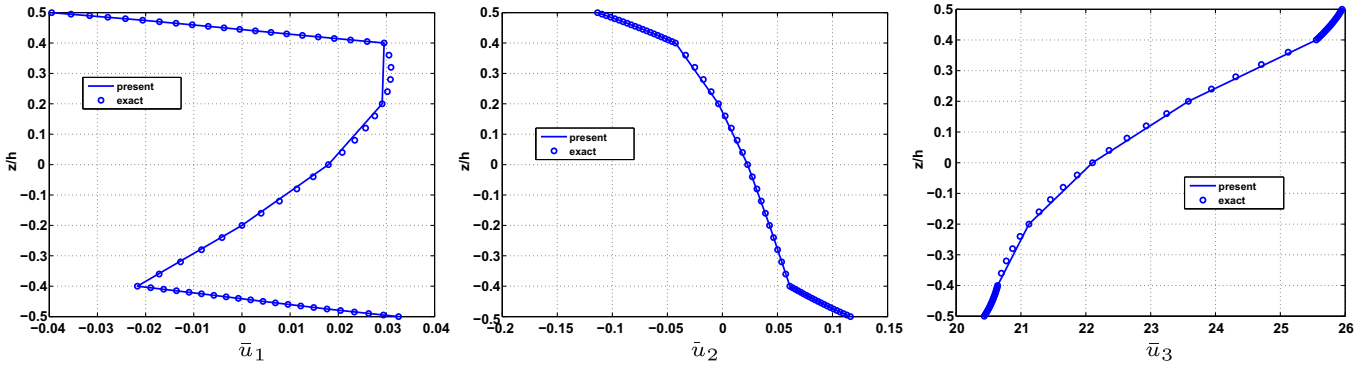

Fig. 14. Distribution of $\bar{u}_1$ (left), $\bar{u}_2$ (middle) and $\bar{u}_3$ (right) along the thickness – $S = 2$ – sandwich – $d^{\circ}4$.

shear stresses in the faces is captured. In this example, the compatibility conditions on σ_{i3} are also satisfied.

4.6. Comments about computational cost

This section deals with the computational complexity of the present PGD method. It is compared with a layerwise approach.

By assuming a direct band solver to solve these two types of methods, the estimation of the number of operations, denoted *NbOp*, gives:

- LayerWise approach: $NbOp \sim N_x^3 \times N_y \times Degz^3 \times N_z^3$,
- PGD approach: $NbOp \sim N_x^3 \times N_y \times N_{couple}$,

where *Degz* is the order of expansion of the unknowns with respect to z, N_z is the number of numerical layers, and N_{couple} is the number of couples built in the PGD process. The cost of the 1D problem involving the z functions is neglected. We also assume that $N_x > N_y$. This estimation is suitable when the number of elements $N_x \times N_y$ and N_z are high. It allows us to show that the number of layers and the degree of expansion of z have a major influence on the computational time of the LW approach. On the contrary,

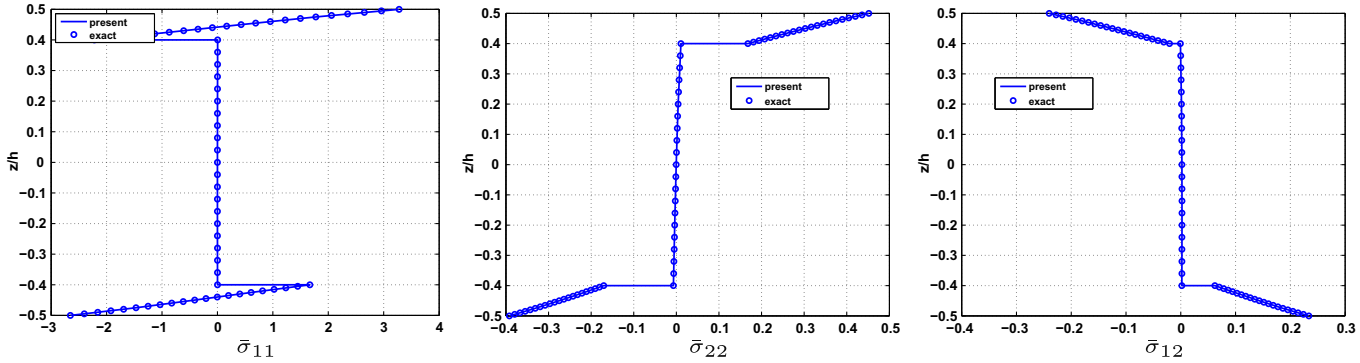

Fig. 15. Distribution of $\bar{\sigma}_{11}$ (left), $\bar{\sigma}_{22}$ (middle) and $\bar{\sigma}_{12}$ (right) along the thickness – $S = 2$ – sandwich – $d°4$.

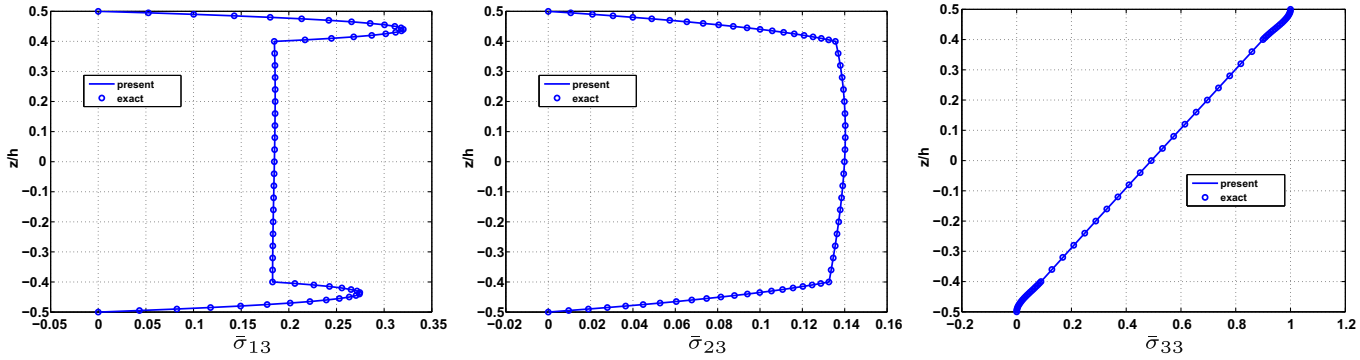

Fig. 16. Distribution of $\bar{\sigma}_{13}$ (left), $\bar{\sigma}_{23}$ (middle) and $\bar{\sigma}_{33}$ (right) along the thickness – $S = 2$ – sandwich – $d°4$.

the PGD approach is not affected by these parameters. This is particularly interesting for the modeling of multi-layered composite structures that exhibit complex behaviour in the thickness direction. So, the most important gain of the PGD approach will be made for complex problems where the number of physical layers increases, i.e. when $Degz^3 \times N_z^3 \gg N_{couple}$.

5. Conclusion

In this article, the PGD is applied to plates modeling using a LW description of the displacements, and the results are assessed through different benchmarks. In particular, the influence of the degree of the z-function to compute the global and local quantities is emphasized. A preliminary study shows that a fourth-order expansion is needed to compute mechanical quantities with accuracy and efficiency. So, this method has been applied to the modeling of laminated and sandwich composite plates. Accurate results are obtained for very thick to thin plates under uniform and localized mechanical loading. This study has shown the ability of the approach to capture local effects and complex distributions of displacements and stresses through the thickness induced by the loading, the stacking sequences or the type of composite plates. Moreover, in the case of complex layered structures, the present method is much less costly than layerwise FE approach and allows to refine the transverse behaviour with very few additional computational times.

Based on these promising results, the use of the PGD for layerwise shell FE will be carried out.

References

Ambartsumyan, S., 1969. In: Ashton, J.E. (Ed.), Theory of Anisotropic Plates. Technomic Publishing Co. (Translated from Russian by T. Cheron).

Ammar, A., Mokdada, B., Chinesta, F., Keunings, R., 2006. A new family of solvers for some classes of multidimensional partial differential equations encountered in kinetic theory modeling of complex fluids. J. Non-Newtonian Fluid Mech. 139, 153–176.

Bognet, B., Bordeu, F., Chinesta, F., Leygue, A., Poitou, A., 2012. Advanced simulation of models defined in plate geometries: 3d solutions with 2d computational complexity. Comput. Methods Appl. Mech. Eng. 201-204, 1–12, doi: http://dx.doi.org/10.1016/j.cma.2011.08.025.

Carrera, E., 1999. A study of transverse normal stress effect on vibration of multilayered plates and shells. J. Sound Vib. 225, 803–829.

Carrera, E., 2000. A priori vs. a posteriori evaluation of transverse stresses in multilayered orthotropic plates. Compos. Struct. 48 (4), 245–260.

Carrera, E., 2002. Theories and finite elements for multilayered, anisotropic, composite plates and shells. Arch. Comput. Methods Eng. 9, 87–140.

Carrera, E., 2003. Historical review of zig-zag theories for multilayered plates and shells. Appl. Mech. Rev. 56 (3), 287–308.

Cook, G., Tessler, A., 1998. A {3,2}-order bending theory for laminated composite and sandwich beams. Compos. Part B: Eng. J. 29B, 565–576.

Demasi, L., 2008. ∞^3 plate theories for thick and thin plates: the generalized unified formulation. Compos. Struct. 84, 256–270.

Ferreira, A., 2005. Analysis of composite plates using a layerwise shear deformation theory and multiquadrics discretization. Mech. Adv. Mater. Struct. 12, 99–112.

Icardi, U., 2001. Higher-order zig-zag model for analysis of thick composite beams with inclusion of transverse normal stress and sublaminates approximations. Compos. Part B: Eng. J. 32, 343–354.

Kant, T., Swaminathan, K., 2002. Analytical solutions for the static analysis of laminated composite and sandwich plates based on a higher order refined theory. Compos. Struct. 56, 329–344.

Kapuria, S., Dumir, P., Ahmed, A., 2003. An efficient higher order zig-zag theory for composite and sandwich beams subjected to thermal loading. Int. J. Solids Struct. 40, 6613–6631.

Kim, J.-S., Cho, M., 2007. Enhanced first-order theory based on mixed formulation and transverse normal effect. Int. J. Solids Struct. 44, 1256–1276.

Lee, C.-Y., Liu, D., Lu, X., 1992. Static and vibration analysis of laminated composite beams with an interlaminar shear stress continuity theory. Int. J. Numer. Methods Eng. 33, 409–424.

Librescu, L., 1967. On the theory of anisotropic elastic shells and plates. Int. J. Solids Struct. 3, 53–68.

Lo, K., Christensen, R., Wu, F., 1977. A higher-order theory of plate deformation. Part II: Laminated plates. J. Appl. Mech. ASME 44, 669–676.

Matsunaga, H., 2002. Assessment of a global higher-order deformation theory for laminated composite and sandwich plates. Compos. Struct. 56, 279–291.

Noor, A., Burton, W., 1990. Assessment of computational models for multilayered composite shells. Appl. Mech. Rev. 43 (4), 67–97.
Nouy, A., 2010. A priori model reduction through proper generalized decomposition for solving time-dependent partial differential equations. Comput. Methods Appl. Mech. Eng. 199 (23–24), 1603–1626.
Pagano, N., 1969. Exact solutions for composite laminates in cylindrical bending. J. Comput. Mater. 3, 398–411.
Pagano, N., 1970. Exact solutions for rectangular bidirectional composites and sandwich plates. J. Comput. Mater. 4, 20–34.
Polit, O., Vidal, P., D'Ottavio, M., 2012. Robust c^0 high-order plate finite element for thin to very thick structures: mechanical and thermo-mechanical analysis. Int. J. Numer. Methods Eng. 40, 429–451. http://dx.doi.org/10.1002/nme.3328.
Rao, M., Desai, Y., 2004. Analytical solutions for vibrations of laminated and sandwich plates using mixed theory. Compos. Struct. 63, 361–373.
Reddy, J., 1984. A simple higher-order theory for laminated composite plates. J. Appl. Mech. ASME 51 (4), 745–752.
Reddy, J., 1989. On refined computational models of composite laminates. Int. J. Numer. Methods Eng. 27, 361–382.
Reddy, J., 1997. Mechanics of Laminated Composite Plates – Theory and Analysis. CRC Press, Boca Raton, FL.
Savoia, M., Reddy, J., 1992. A variational approach to three-dimensional elasticity solutions of laminated composite plates. J. Appl. Mech. ASME 59, 166–175.
Sciuva, M.D., Icardi, U., 2001. Numerical assessment of the core deformability effect on the behavior of sandwich beams. Compos. Struct. 52, 41–53.
Shimpi, R., Ainapure, A., 2001. A beam finite element based on layerwise trigonometric shear deformation theory. Compos. Struct. 53, 153–162.
Tanigawa, Y., Murakami, H., Ootao, Y., 1989. Transient thermal stress analysis of a laminated composite beam. J. Therm. Stresses 12, 25–39.
Vidal, P., Polit, O., 2008. A family of sinus finite elements for the analysis of rectangular laminated beams. Compos. Struct. 84, 56–72. http://dx.doi.org/10.1016/j.compstruct.2007.06.009.
Vidal, P., Polit, O., 2009. A refined sine-based finite element with transverse normal deformation for the analysis of laminated beams under thermomechanical loads. J. Mech. Mater. Struct. 4 (6), 1127–1155.
Vidal, P., Polit, O., 2011. A sine finite element using a zig-zag function for the analysis of laminated composite beams. Compos. Part B: Eng. J. 42 (6), 1671–1682. http://dx.doi.org/10.1016/j.compositesb.2011.03.012.
Vidal, P., Gallimard, L., Polit, O., 2012a. Assessment of a composite beam finite element based on the proper generalized decomposition. Compos. Struct. 94 (5), 1900–1910. http://dx.doi.org/10.1016/j.compstruct.2011.12.016.
Vidal, P., Gallimard, L., Polit, O., 2012b. Composite beam finite element based on the proper generalized decomposition. Comput. Struct., 76–86. http://dx.doi.org/10.1016/j.compstruc.2012.03.008.
Whitney, J., 1969. The effect of transverse shear deformation in the bending of laminated plates. J. Comput. Mater. 3, 534–547.
Whitney, J., Sun, C., 1973. A higher order theory for extensional motion of laminated composites. J. Sound Vib. 30, 85–97.
Yang, P., Norris, C., Stavsky, Y., 1966. Elastic wave propagation in heterogeneous plates. Int. J. Solids Struct. 2, 665–684.
Zhang, Y., Yang, C., 2009. Recent developments in finite elements analysis for laminated composite plates. Compos. Struct. 88, 147–157.